Journal of Materials Chemistry B

Accepted Manuscript

ROYAL SOCIETY OF CHEMISTRY

www.rsc.org/materialsB

Journal of Materials Chemistry B RSCPublishing

ARTICLE

Mussel-inspired polydopamine coating as a versatile platform for synthesizing polystyrene/Ag nanocomposite particles with enhanced antibacterial activities

Cite this: DOI: 10.1039/xoxxoooooox

Received ooth January 2014,
Accepted ooth January 2014

DOI: 10.1039/xoxxoooooox

www.rsc.org/

Ying Cong,[§a] Tian Xia,[§b] Miao Zou,[§b] Zhenni Li,[a] Bo Peng,[*c] Dingzong Guo[*b] and Ziwei Deng[*a]

Inspired by mussel-adhesion phenomena in nature, we present a simple, mild and green method to prepare polystyrene/Ag (PS/Ag) nanocomposite particles with enhanced antibacterial activities. In this approach, monodisperse polystyrene particles are used as template spheres, which is then coated with polydopamine (PDA) through the self-polymerization of dopamine in a weakly alkaline aqueous environment (pH = 8.5). Silver precursor-$[Ag(NH_3)_2]^+$ ions are added and absorbed onto the surfaces of the PS/PDA composite spheres by the active catechol and amine groups of the polydopamine coating. Meanwhile, these adsorbed $[Ag(NH_3)_2]^+$ ions are *in situ* reduced into metallic silver nanoparticles by the "bridge" of the polydopamine coating, and the formed Ag nanoparticles are home positioned. Since polydopamine is an environmentally friendly reagent with abilities as a universal adhesive to any surfaces and as a mild reductant for noble metal salts, due to its abundant active catechol and amine groups, neither additional reducing and toxic reagents nor special surface modifications of the template are needed in this procedure. Moreover, the preliminary antibacterial assays indicate that these PS/Ag nanocomposite particles show the enhanced antibacterial activities against *Escherichia coli* (Gram-negative bacteria) and *Staphylococcus aureus* (Gram-positive bacteria), while, they do not show a significant *in vitro* cytotoxicity against HEK293T human embryonic kidney cells. These results allow these PS/Ag nanocomposite particles as a promising antibacterial materials for future biomedical applications.

1. Introduction

The outbreaks of infectious diseases caused by various pathogenic bacteria and the risk of new resistant strains of bacteria to current antibiotics, have greatly threaten the public health in recent years. Therefore, much attention has been focused on creating new and effective antibacterial agents to meet the increasing general demands for hygiene in public health care.[1-4]

Recently, nano-structured materials as novel antibacterial agents have been considered as promising candidates for biomedical applications, owing to their uniquely physical, chemical and biological properties.[1, 2] Many kinds of nano-structured materials such as TiO_2,[5] ZnO,[6] copper,[7] gold[8] and silver[1, 2] have been intensively investigated. Among them, silver-based nanomaterials have been extensively used as effective antimicrobial agents against a wide range of microorganisms (e.g. bacteria,[9, 10] fungi and virus[11]), due to its relatively low toxicity to humans.[12, 13] Although, silver and its

[a] *School of Materials Science and Engineering, Shaanxi Normal University, Xi'an,710062, China. E-mail: zwdeng@snnu.edu.cn; Tel:+86-29-81530804; Fax: +86-29-81530702.*
[b] *College of Veterinary Medicine, Huazhong Agricultural University, Wuhan, 430070, China. E-mail:hlgdz@163.com; Tel:+86-27-87285859. Fax: +86-27-87280408.*
[c] *Soft Condensed Matter, Debye Institute for NanoMaterials Science, Utrecht University, Princetonplein 5,3584 CC, Utrecht, the Netherlands. Email:b.peng@uu.nl; Tel:+31-30-253320.Fax:+31-30-2532706.*
[§] These three authors contributed equally to this work.
†Electronic Supplementary Information (ESI) available. See DOI: 10.1039/b000000x/

salts have been well known as antibacterial agents for the treatment of the infections, burns and chronic wounds in curative and preventive health care for centuries, the detailed antimicrobial mechanisms of silver are still not fully understood. Recent investigations have suggested that Ag nanoparticles themselves could directly react with those sulfur-containing proteins inside or outside the cell membrane of the bacteria, which straightly cause the structural changes or functional damages to the cell membrane of the bacteria, and further affect the viability of the bacterial cells.[9, 14] In addition, the released Ag ions (particularly, Ag^+) from the Ag nanoparticles can also deactivate microorganism cells to death by interacting with the disulfide or sulfhydrol groups of the enzymes, and further causing the structural changes and destroying the metabolic process of bacterial cells.[15, 16]

However, the practical applications of the Ag nanoparticles are frequently hampered by the ease of oxidization and aggregation of them, which cause a quick loss of the antibacterial activities of the Ag nanoparticles. Because the antibacterial activities of the Ag nanoparticles strongly depend on their sizes at nanometer scales. The smaller the particle sizes are, the better their antibacterial activities will perform. Therefore, the aggregation of the Ag nanoparticles will cause antibacterial activities to be diminished or even lost.[17-19] To overcome this shortcoming, the incorporation of the Ag nanoparticles into/onto various matrices is an effective way, which has been intensively investigated to enhance the stability and antibacterial activity of the Ag nanoparticles. For instance, various kinds of materials including polymers,[20, 21] silica,[22] iron oxides,[23] titanium oxide,[24] carbon nanotubes[25, 26] and carbonaceous materials,[27] have been commonly used as the substrates to load Ag nanoparticles. Although the load of the Ag nanoparticles onto these substrates materials can effectively enhance the stability and antibacterial activity of the Ag nanoparticles, the complicated and tedious synthetic strategies with some certain reagents such as surfactants, stabilizers and reducing agents [28-30] are required in these preparation processes, which usually result in much time and finance consumption in the practical applications. On the other hand, the usage of unbiocompatible and hazardous reductants or the introduction of the groups which electrostatically or chemically locate Ag ions at the surface of the substrates in these strategies can potentially lead to a toxicity for the environment or biological hazard for the living cells.[12, 31-33] Therefore, an straightforward and environmentally friendly synthetic strategy for the preparation of the Ag nanocomposite materials is highly desired in view of the increasing demands from the potential biomedical applications.

Inspired by mussel-adhesion phenomena in nature, dopamine (DA), a biomolecule which contains catechol and amine functional groups can mimic the powerful adhesive foot protein, Mefp-5 (Mytilus edulis foot protein 5) secreted by mussels. Generally, under the weak alkaline aqueous conditions and in the presence of oxygen at room temperature, dopamine can self-polymerize into polydopamine (PDA) which spontaneously deposits a thin adherent coating on various material surfaces, which shows a similar character to the adhesive foot proteins secreted by mussels.[34, 35] More importantly, these formed adherent polydopamine coatings with a surface having ample of active catechol and amine groups, which is able to serve as the reductants, binding reagents and universal platforms for the secondary reactions.[34] Recently, thank to these advantageous features of polydopamine coatings, a diversity of metallic nanoparticles have been introduced onto various substrates via the reduction of the metal ions. Additionally, similar to the nature adhesive protein, PDA demonstrates a good biocompatibility and low toxicity for the environment.[36-39] Hence, the usage of polydopamine as a coating or/and surface modification reagent can offer an simple and environmentally friendly approach to *in situ* bridge the metal nanoparticles with various substrate under a mild reaction conditions in the absence of any expensive or toxic ingredients, or using intricate instruments. These advanced characters would be helpful for the future commercial production and application.

Herein, we present an easy, mild and green approach to prepare polystyrene/silver (PS/Ag) nanocomposite particles with enhanced antibacterial activities. In this approach, monodisperse polystyrene particles were used as template spheres, and with a subsequent coating step by polydopamine through the self-polymerization of dopamine in a weakly alkaline aqueous environment. Subsequently, silver precursor-$[Ag(NH_3)_2]^+$ ions aqueous solution was successfully *in situ* reduced to silver nanoparticles (Ag NPs) by polydopamine coating, and they were deposited on the surface of the polystyrene/polydopamine (PS/PDA) composite spheres. This approach is also called polydopamine-assisted electroless Ag

metallization, which possesses three highlighted unique characteristics: (1) the coating of polydopamine is carried out under a very mild and easy conduction condition without any pre-treatments of the surface of the polystyrene template spheres or co-polymerization with extra co-monomers during the synthesis of template PS spheres; (2) the formed adherent polydopamine coatings have abundant of active catechol and amine groups on the surface, which facilitate the secondary reaction and further decoration of the surface. Moreover, these ample amounts of functional groups of polydopamine coatings provide an excellent platform to *in situ* bind and reduce silver precursor- $[Ag(NH_3)_2]^+$ ions into metallic Ag nanoparticles on polystyrene spheres. Neither additional reductants nor toxic reagents are needed in this procedure; (3) the coverage and the size of the Ag nanoparticles on the surface of PS/PDA composite spheres can be easily tailored through the adjustment of the concentration of the silver precursor. Therefore, our method inherently offers a simple, mild, environmentally friendly and controllable route for the synthesis of Ag-based nanocomposite particles. In addition, the produced PS/Ag nanocomposite particles can be used as the antibacterial agents against *Escherichia coli* (Gram-negative bacteria) and *Staphylococcus aureus* (Gram-positive bacteria), which exhibited an enhanced antibacterial performance against *Escherichia coli* and *Staphylococcus aureus.*

2. Experimental section

2.1 Materials

Polyvinylpyrrolidone (PVP, MW=40,000 g/mol), 3-Hydroxy-tyramine hydrochloride (Dopamine hydrochloride) and Tris (hydroxymethyl)aminomethane (Tris base, ≥99.8%) were purchased from Sigma-Aldrich and used as received. Styrene (St) was bought from Tianjin Tianli Chemical Reagent Co., Ltd. (China) and was distilled to remove the inhibitor in vacuum, and then stored at 4°C until use. 2, 2'-azobisisobutyronitrile (AIBN) was purchased from Shanghai Chemical Reagent Co. (China) and was purified by recrystallization in ethanol. Hydrochloric acid (HCl, 36 wt% in water), Silver nitrate ($AgNO_3$, ≥99.8%), aqueous ammonia (28 wt% aqueous solution), absolute ethanol were purchased from Sinopharm Chemical Reagent Co., Ltd (China) and used without further purification. Ultrapure water (>17 $M\Omega cm^{-1}$) from a Milli-Q water system was used throughout the experiments.

2.2 Preparation of monodisperse polystyrene spheres

Micron-sized monodisperse polystyrene spheres (PS) were prepared by dispersion polymerization according to our previous work.[40] In brief, all of styrene (10.0 g), PVP (3.0 g), AIBN (0.2 g), ethanol (75.0 g) and water (25.0 g) were added into a 250 mL four-necked round-bottom flask equipped with a mechanical stirrer, a thermometer with a temperature controller, a N_2 inlet, a Graham condenser and a heating mantle. The solution was deoxygenated by bubbling pure nitrogen gas thought the flask at room temperature for ca. 60 min, and then, the flask was heated to 70 °C and the polymerization took place for 24 h under a constant stirring with a rate of 100 rpm. After the complete of reaction, the dispersion was centrifuged and washed with ethanol, and finally, was dried in vacuum oven at room temperature for 24 h.

2.3 Preparation of monodisperse polystyrene/polydopamine (PS/PDA) composite spheres

The process was described as following: In detail, dopamine aqueous solution (2 mg/mL) was first prepared by dissolving dopamine (400 mg) in the Tris–HCl buffer (200 mL, 10 mM; pH = 8.5). Then, the dried PS powder (0.1 g) was immersed into the dopamine solution, and kept magnetically stirring at room temperature. After 36 h, the reaction was complete, and the core-shell structured PS/PDA composite spheres were obtained. These as-prepared PS/PDA composite spheres were separated by centrifugation, and were thoroughly cleaned by ultrasonication and rinse with deionized water several times. The final product was dried for 24 h in a vacuum oven at room temperature.

2.4 Preparation of PS/Ag nanocomposite particles

The typical strategy used to fabricate PS/Ag nanocomposite particles has been illustrated in Scheme 1. As described: first, various concentrations of $[Ag(NH_3)_2]^+$ ions aqueous solutions (0.012 mol/L - 0.094 mol/L) were freshly prepared with an addition of aqueous ammonia into $AgNO_3$ solution until the solution became transparent. Subsequently, 0.1 g of PS/PDA composite spheres was added into 50 mL of freshly prepared $[Ag(NH_3)_2]^+$ ions aqueous solution mentioned above, and the system was magnetically stirred at a speed of 100 rpm at room temperature for 1 h. In this process, $[Ag(NH_3)_2]^+$ ions were first absorbed onto the surfaces of the PS/PDA composite spheres

surfaces due to the catechol and amine groups of the polydopamine shell. Then, these adsorbed $[Ag(NH_3)_2]^+$ ions on the surfaces of polystyrene spheres were *in situ* reduced to the metallic silver nanoparticles by the polydopamine coating, and finally, PS/Ag nanocomposite particles were formed through this so-called electroless metallization procedure.[41 34, 42, 43] The PS/Ag nanocomposite particles were collected via a repeat of centrifugation and washing with an excess amount of deionized water several times, and in the end, they were dried in the vacuum oven at room temperature for 24 h. These as-synthesized PS/Ag nanocomposite particles were collected and stored in vials for further characterization and experiments.

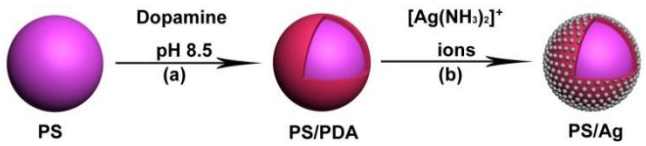

Scheme 1. Schematic diagram illustrating the formation of the PS/Ag nanocomposite particles by polydopamine-assisted electroless Ag metallization.

2.5 Antibacterial assays

For the antibacterial activity assays, two bacterial species, *Escherichia coli* (Gram-negative bacteria) and *Staphylococcus aureus* (Gram-positive bacteria), were used through all experiments. The bacterial suspensions were prepared by taking a single colony from the stock bacterial culture with a loop and inoculating 5 mL of sterile nutrient broth medium, which were then incubated in a shaking incubator (37 ℃ at 200 rpm) for 12 h. Later, 30 μL of bacterial suspensions (O.D.=0.6) were inoculated in a 3 mL of liquid nutrient broth medium supplemented with different concentrations of PS/Ag nanocomposite particles. The suspensions were shaken by a shaker at 200 rpm under 37 ℃, and their bacterial survivals were determined by measuring the optical density (O.D.) of the nutrient broth in both medium at a wavelength of 600 nm. The absorbance was sequentially checked from time 0 to 10 h with an interval of 1 h. In addition, the commercial antibiotic kanamycin was selected as the positive control groups to compare the antibacterial activities against *Escherichia coli* and *Staphylococcus aureus*. The procedure for their antibacterial activity assays was the same with just mentioned above.

To further examine the antibacterial properties, the bacteria were staining with the live/dead Bacterial Viability Kit following the protocol (GENMED). Briefly, 3 μL of the fluorescently-dyed mixture was added into each milliliter of the bacterial suspensions. Then, these sample was thoroughly mixed and incubated at room temperature in the dark for 15 minutes. In order to observe and image with a Fluorescence Microscope (Olympus IX71), 5 μL of the stained bacterial suspension was added between a slide and a square cover slip.

2.6 Cell culture

HEK293T human embryonic kidney cells were kindly donated by Professor Shaobo Xiao (Huazhong Agricultural University, China) and routinely cultured at 37°C and 5% CO_2 atmosphere in the Dulbecco's Modified Eagle Medium (Hyclone) supplemented with 10% fetal bovine serum (Hyclone), Penicillin-Streptomycin solution (100U/mL, 100μg/mL, Beyotime). They were seeded with an equal density in each well in 96-well plates (1×10^4 cells per well) in a 100 μL of Dulbecco's Modified Eagle medium (DMEM) supplemented with 10% fetal bovine serum (FBS) for 24 h at 37 °C under a humidified 5% CO_2-containing atmosphere and grew overnight prior to further studies.

2.7 *In vitro* cytotoxicity and cell viability evaluation

The *in vitro* cytotoxicity of PS/Ag nanocomposite particles against HEK293T human embryonic kidney cells was tested by using the Cell Counting Kit-8 assay (CCK-8, Dojindo, Japan). CCK-8 is based on the colorimetric assays with the highly water tetrazolium salt, WST-8 [2-(2-methyxy-4-nitrophenyl)-3-(4-nitrophenyl)-5-(2, 4-disulfophenyl)-*2H*-tetrazolium, mono sodium salt]. Specifically, the HEK293T human embryonic kidney cells were seeded in 96-well plates with a density of 1×10^4 cells/well in the 100 μL of Dulbecco's Modified Eagle medium (DMEM) supplemented with 10% fetal bovine serum (FBS) and cultured under a humidified atmosphere of 5% CO_2 at 37 °C for 24 h prior to the exposure to the above materials. Then, the HEK293T human embryonic kidney cells were incubated in the growth medium containing different concentrations (2, 4, 8, 12 and 16 μg/mL) of PS/Ag nano composite particles in the growth medium for another 24 h. Meanwhile, the wells only containing the cell medium were also prepared as the untreated controls. Subsequently, 10 μL of CCK-8 dye was added to each well and the plates were incubated for another 2 h at 37 °C. The absorbance was measured with the single wavelength spectrophotometry at 450 nm by using a microplate reader (Bio-Rad 680). The

experimental results were expressed as mean values of three measurements, and the relative cell viability (%) was determined by comparing the absorbance at 450 nm with the control wells containing only the cell culture medium.

2.8 Characterization

TEM observation Transmission electron microscopy (TEM, JEOL JEM-2100, Japan) was used to observe the morphologies of obtained spheres (PS spheres, PS/PDA composite spheres and PS/Ag nanocomposite particles). All samples were diluted with ethanol, ultrasonicated at 25 ^{o}C for 10 min, and dried onto the carbon-coated copper grids prior to examination. The average diameter of the particles was calculated by averaging more than 100 particles in the TEM images.

SEM observation Scanning electron microscopy (SEM, Hitachi S-4800, Hitachi, Ltd. Japan,) was used to characterize the surface morphologies of the PS spheres, PS/PDA composite spheres and PS/Ag nanocomposite particles. All dispersions were diluted with ethanol and dried on the silica wafers at room temperature before observation.

X-ray diffraction Powder X-ray diffraction was performed on a DX-2700 X-ray diffractometer equipped with a Cu tube and a diffracted beam curved graphite monochromator operating at 40 kV and 30 mA. Crystal structure identification was carried out by scanning the PS/Ag powders deposited on a glass substrate with a scanning rate of 0.02 degrees (2θ) per second in the range of 20 ° and 90 ° (2θ).

X-ray photoelectron spectroscopy X-ray photoelectron spectroscopy (XPS) measurement was carried out on AXIS Ultra X-ray photoelectron spectrometer (Kratos Analytical Ltd. U.K.) equipped with a monochromatized Al Kα X-ray source (1486.6eV). All binding energies were calibrated by using the containment carbon (C1s = 284.6eV).

FTIR Measurement Fourier-transform infrared spectra of PS spheres and PS/PDA composite spheres were recorded on Transform Infrared Spectroscopy (FTIR, EQUINX55, Brucher Crop, Germany). All samples were centrifuged and washed with absolute ethanol. Subsequently, they were dried in a vacuum oven for 24 h and pressed into KBr pellets for the FTIR measurement. The spectra were taken from 4000 to 500 cm^{-1}.

TG analysis The thermogravimetric analysis (TGA) was performed on SDT Q600 (TA Instruments. U.S.A.). All dried powder samples (PS spheres, PS/PDA composite spheres and PS/Ag nanocomposite particles) were heated from 30 ^{o}C to 800 ^{o}C with a rate of 10 ^{o}C/min under nitrogen atmosphere with a flow rate of 50 mL/min.

3. Results and discussion

3.1 Preparation and characterization of PS and PS/PDA composite spheres

The monodisperse template polystyrene (PS) spheres were prepared by dispersion polymerization according to our previous work.[40] As shown the TEM image in Fig. 1a and b, it is confirms that the original PS spheres prepared by dispersion polymerization are uniform at a large scale with an average diameter of 625 nm (by averaging 100 particles in the TEM micrographs). Moreover, the smooth surfaces of the original PS spheres are also confirmed with a high magnification TEM image of one typical PS sphere (see Fig. 1b). Therefore, these monodisperse PS spheres with smooth surfaces are ideal starters for the fabrication of nanocomposites or hollow spheres at a commercial scale. [40, 44-49]

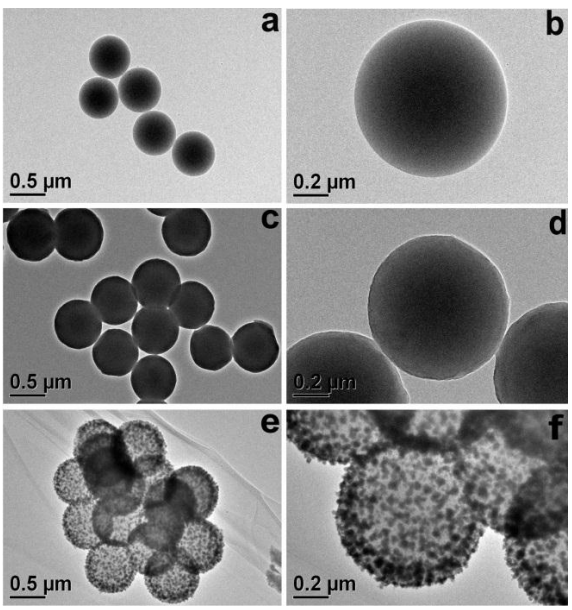

Fig.1 Transmission electron microscopy (TEM) images of (a and b) PS spheres, (c and d) PS/PDA composite spheres and (e and f) PS/Ag nanocomposite particles (PS/PDA composite spheres: 0.1 g; $[Ag(NH_3)_2]^+$ ions: 4.7×10^{-2} mol/L in 50mL aqueous solution; Time: 1h; Temperature: room temperature). The high magnification TEM images in (b), (d) and (f) show the typical PS spheres, PS/PDA composite spheres and PS/Ag nanocomposite particles, respectively.

The surface modification of PS template spheres with dopamine has been illustrated in Scheme 1a. In this process,

monodisperse PS spheres were first dispersed in aqueous Tris-HCl buffer solution, and then, mixed with dopamine (2 mg of dopamine per milliliter of 10 mM Tris-HCl, pH = 8.5). Under the weakly alkaline aqueous conditions and along with oxygen present in the air, dopamine self-polymerize to form a thin adherent polydopamine coatings on the surfaces of the PS template spheres.[34] Note, the PS spheres served as a substrate is not vital, because it has been already proved that polydopamine polymerized from dopamine was able to attach on a variety of substrates without restriction on the type of the materials and the morphologies of the surfaces.[34] This opens a new window for our future research on the abundant selection of the materials[50, 51] and the shapes of the substrates.[52, 53 54] The morphology of the PS/PDA composite spheres was examined by TEM, as shown in Fig. 1c, which clearly indicates that the polydopamine coatings do not have a significant influence on the spherical shape of the PS spheres. While, in comparison with the original PS spheres (see Fig. 1a and b, also see Fig. 4a and b), both of the average size and surface roughness of PS/PDA composite spheres (see Fig. 1c and d) are increased. After coating, the average size of the obtained PS/PDA composite spheres is increased from 625 to 660 nm (by averaging 100 particles in the TEM micrographs). Hence, a thin layer (35 nm) of polydopamine coatings have been successfully formed on the PS template spheres, which paves a way for the further surface decoration through the surface active catechol and amine groups of the PDA shell.[34]

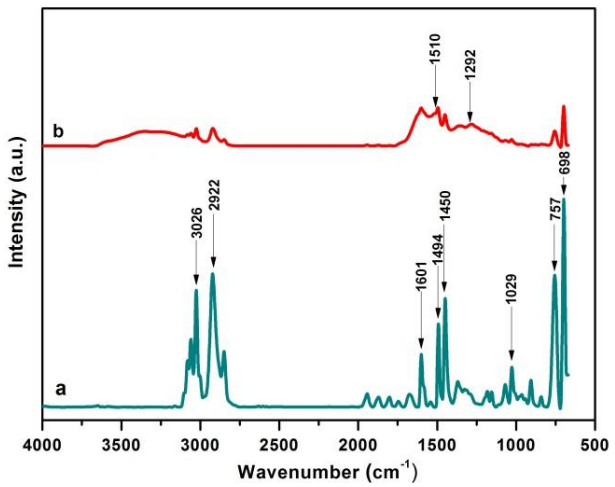

Fig.2 Fourier-transform IR (FTIR) spectra of (a) PS spheres and (b) PS/PDA composite spheres with their characteristic absorption peaks.

Thin polydopamine coatings formed on the surfaces of PS template spheres were also confirmed with the comparison of the Fourier-transform infrared spectra (FTIR) of the PS template spheres and PS/PDA composite spheres (see Fig. 2). Before the surface modification with polydopamine, the typical polystyrene absorption bands at around 698, 757, 1029, 1450, 1494, 1601, 2922 and 3026 cm^{-1} can be clearly seen in the FTIR spectrum of the PS template spheres (Fig. 2a). After the surface covered with polydopamine, several new absorbance signals appear, as shown in Fig. 2b. The broad absorbance between 3600 and 3100 cm^{-1} is ascribed to N-H/O-H stretching vibrations from polydopamine, and the peaks at 1510 cm^{-1} and 1292 cm^{-1} are assigned to the amide N–H shearing vibration and the phenolic C-OH stretching vibration of the polydopamine, respectively.[55-57] These sufficient FTIR results, again, confirm the successful incorporation of the surface-adherent polydopamine coatings on the surfaces of PS template spheres after dopamine self-polymerization.

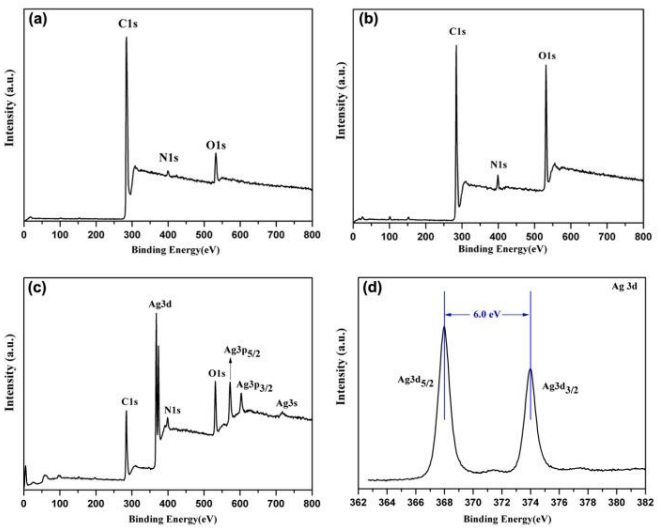

Fig.3 XPS scans of (a) PS spheres; (b) PS/PDA composite spheres; (c) PS/Ag nanocomposite particles and (d) Ag3d core–level spectrum of the PS/Ag nanocomposite particles (PS/PDA composite spheres: 0.1 g; $[Ag(NH_3)_2]^+$ ions: 4.7×10^{-2} mol/L in 50 mL of aqueous solution; Time: 1 h; Temperature: room temperature).

Before coating with silver nanoparticles, XPS spectroscopy was employed to analyze the surface chemical composition of the PS template spheres and PS/PDA composite spheres, respectively. As shown in Fig.3a, the main C1s peak accompanying with the lower intensities of O1s peak and N1s peak are observed in the XPS scan data of the PS template spheres. The appearances of O1s and N1s peaks with low

intensities are attributed to the agents (PVP stabilizer and AIBN initiator) introduced during dispersion polymerization. After the polydopamine coatings on the surfaces of PS template spheres have been formed, the intensities of N1s and O1s peaks are extensively enhanced in the XPS wide scan data of the PS/PDA composite spheres (see Fig. 3b). Carefully comparing the XPS data in Fig. 3a and Fig. 3b, one can observe that the surface O/C mole ratio of the PS/PDA composite spheres is higher than that of the PS template spheres, which is ascribed that the rich oxygen gradient polydopamine coatings have been successfully connected to the surfaces of PS template spheres.[58] Therefore, all evidences demonstrate a success of the preparation of PS/PDA core-shell composite spheres via a self-polymerization of dopamine with monodisperse PS template spheres.

3.2 Preparation and characterization of PS/Ag nanocomposite particles

The preparation procedures of the PS/Ag nanocomposite particles through polydopamine-assisted electroless Ag metallization is shown in Scheme 1b. After the self-polymerization of dopamine in the basic environment, the thin polydopamine coatings have been homogeneously deposited on the surfaces of PS template spheres, in the other word, led to a core-shell structured PS/PDA composite spheres. Subsequently, the as-prepared core-shell PS/PDA composite spheres were dispersed into the $[Ag(NH_3)_2]^+$ ions aqueous solution to decorate Ag nanoparticles. In this process, the polydopamine coatings were served as a bridge between PS spheres and $[Ag(NH_3)_2]^+$ ions, and *in situ* reduced the $[Ag(NH_3)_2]^+$ into Ag nanoparticles, with the help of the catechol and amine groups of the polydopamine coatings. During this process, neither extra surface modifications nor auxiliary reductants were needed. Furthermore, polydopamine is also a biocompatible material with which the environmentally friendly materials can be developed then.

Fig. 1e displays the TEM image of the PS/Ag nanocomposite particles through this polydopamine-assisted electroless Ag metallization method. In comparison with PS template spheres (Fig. 1a) and PS/PDA composite spheres (Fig. 1c), those PS/Ag nanocomposite particles are of relatively rough surfaces, and a huge contrast between PS/PDA and Ag nanoparticles can be obviously observed, all of which evidence that Ag nanoparticles have been formed and deposited on the PS/PDA composite spheres in aid of the polydopamine intermedia. The high magnification TEM image (see Fig.1f) illustrates that the uniform Ag nanoparticles homogeneously distribute on the surfaces of PS spheres, which also hints that the polydopamine layer is uniformly growing on top of the PS spheres, excluding the formation of the eccentric core-shell structure.[59-61]

Similarly, the chemical information of the surface of the PS/Ag nanocomposite particles was also examined by XPS analysis. As shown in Fig.3c, C1s, N1s, O1s, Ag3d, Ag3p ($Ag3p_{5/2}$, $Ag3p_{3/2}$) and Ag3s signal peaks distinctly exist in the XPS wide scan data of PS/Ag nanocomposite particles, in which the strong Ag signal peaks at a binding energy of about 370.0 eV strongly demonstrate the emergence of the silver element. Closely inspection of the XPS spectrum of Ag3d, as shown in Fig. 3d, exhibits two peaks at 368.0 eV and 374.0 eV which correspond to the binding energies of the Ag $3d_{5/2}$ and Ag $3d_{3/2,}$ respectively, with a spin-orbit separation of 6.0 eV. Both of the $Ag3d_{5/2}$(368.0 eV) and $Ag3d_{3/2}$(374.0 eV) characteristic peaks are attributed to the Ag^0 species, which certainly indicate the formation of metallic silver existing at zero valent state in the system.

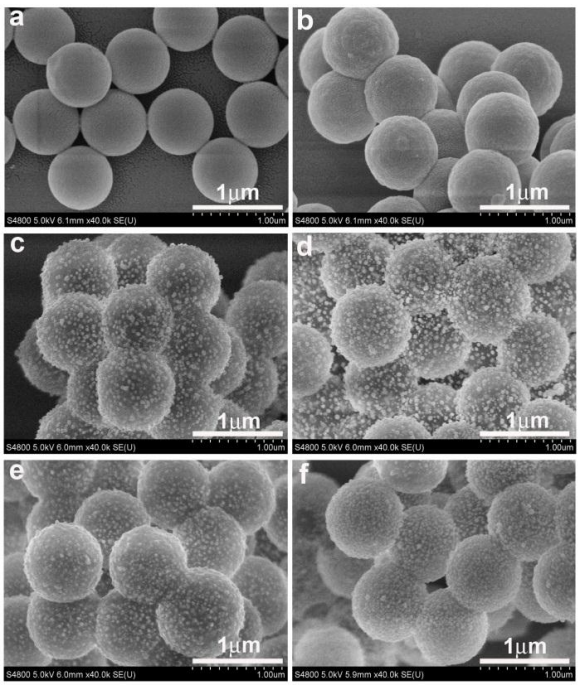

Fig.4 Scanning electron microscopy (SEM) images of (a) PS spheres, (b) PS/PDA composite spheres and (c-f) PS/Ag nanocomposite particles prepared by using various concentrations of $[Ag(NH_3)_2]^+$ ions: (c) 1.2×10^{-2} mol/L; (d) 2.3×10^{-2} mol/L; (e) 4.7×10^{-2} mol/L and (f) 9.4×10^{-2} mol/L. PS/PDA composite particles: 0.1 g; $[Ag(NH_3)_2]^+$ ions in 50 mL of aqueous solution; Time: 1 h; Temperature: room temperature.

3.3 Effect of the concentration of $[Ag(NH_3)_2]^+$ ions

In our green synthetic strategy of the Ag nanoparticles attached at the surface of the micron-sized PS/PDA composite spheres, the concentration of $[Ag(NH_3)_2]^+$ ions plays a vital role in the size and morphology control of the aimed particles. As just mentioned, PS/PDA composite spheres enable to *in situ* reduce $[Ag(NH_3)_2]^+$ ions to Ag nanoparticles and exclusively bond them at the outer PDA layer (see Fig. 4b-f) with the help of the abundant catechol and amine groups of the PDA. With a constant amount of the active groups of the PDA, the average size of the Ag nanoparticles declines as increasing the content of the $[Ag(NH_3)_2]^+$ ions, which was confirmed by the scanning electron microscopy images (SEM) (see Fig. 4c-f). However, from these SEM images, the uniformity and size of the Ag nanoparticles can be roughly estimated. Although the exact polydispersities of the Ag nanoparticles cannot be measured due to the limitation of the current characterization, it still impresses a clear tendency of the improvement in polydispersity and size decrease of the Ag nanoparticles, as shown in Fig. 4c-f, as the concentration of the $[Ag(NH_3)_2]^+$ ions increase.

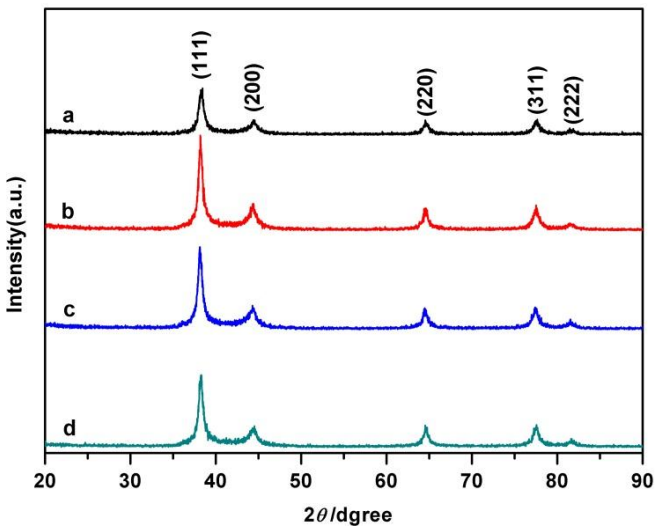

Fig.5 X-ray diffraction (XRD) patterns of the PS/Ag nanocomposite particles prepared by using various concentrations of $[Ag(NH_3)_2]^+$ ions: (a) 1.2×10^{-2} mol/L, (b) 2.3×10^{-2} mol/L, (c) 4.7×10^{-2} mol/L and (d) 9.4×10^{-2} mol/L. PS/PDA composite particles: 0.1 g; $[Ag(NH_3)_2]^+$ ions: 50 mL aqueous solution; Time: 1 h; Temperature: room temperature.

In order to determine the exact size of the obtained Ag nanoparticles, XRD is an indirect, but powerful tool, the secondary function of which is to explore the crystal structure of the product. First, these PS/Ag nanocomposite particles prepared at the various concentrations of $[Ag(NH_3)_2]^+$ ions (1.2×10^{-2}-9.4×10^{-2} mol/L) were examined by XRD to ascertain the crystal structure of the Ag nanoparticles coated on the PS/PDA composite spheres. All the typical XRD patterns of the PS/Ag nanocomposite particles have been illustrated in Fig. 5, which exhibits the peaks at 2θ angles of 37.9°, 44.1°, 64.3°, 77.2° and 81.4° corresponding to the reflections of (111), (200), (220), (311) and (222) crystalline planes of the *fcc* structure of Ag (JCPDS No.04-0783). These results indicate that Ag nanoparticles with *fcc* crystal structure can be obtained through our method. Second, the strongest characteristic reflection (111) of Ag can be used to estimate the average crystallite size of the Ag nanoparticles according to the Scherrer formula, by which the average sizes of the Ag nanoparticles on PS/Ag nanocomposite particles prepared at the various concentrations of $[Ag(NH_3)_2]^+$ ions (1.2×10^{-2}-9.4×10^{-2} mol/L) can be calculated. A good agreement with previous SEM observation, the average size of the Ag nanoparticles first increases from 11.0 to 14.5 nm, and then, decreases to 11.2 and further to 10.5 nm, as the concentration of the $[Ag(NH_3)_2]^+$ ions increases from 1.2×10^{-2} to 2.3×10^{-2} and 4.7×10^{-2}, and finally to 9.4×10^{-2} mol/L, correspondingly.

LaMer and his colleagues pioneeringly proposed the "burst nucleation" which is ideally elucidate our shown results.[62 63] They believed that the final size of the nanoparticles was mainly determined by the supersaturation of the initial concentration of the precursor. Once the degree of the supersaturation is high enough to overcome the energy barrier for nucleation, the nuclei with a minimum radius (it is called critical radius r_c) that can grow spontaneously in the supersaturated solution are formed. Thus, the supersaturation of the precursor is dramatically declined, which directly switches the system into growth stage. If at the end of the nucleation stage, the supersaturation is too low for all the particles to keep growing, particles smaller than r_c dissolve and this precursor diffuse toward larger particles and precipitate on them (this is known as Ostwald ripening). On the other hand, a higher initial supersaturation of precursor results in the formation of more stable nuclei that can mature to nanoparticles in the end, and further grow to more monodisperse but smaller nanoparticles.[64-66] Based on these results, a promising extension of preparation of monodisperse silver nanoparticles with a controllable size

and polydispersity can be developed in the following exploration.

In Fig. 6, the thermal stability of various as-synthesized particles (PS spheres, PS/PDA composite spheres and PS/Ag nanocomposite particles) was studied by thermogravimetric analysis (TGA). The pure PS spheres start to loss their weight at around 300 ^{o}C, and the weight percent of its residue became constant at about 0% after the elevation of the temperature to 430 ^{o}C. Although, in principal, the PS spheres should be converted to carbon under the anaerobic circumstances at a high temperature (800 ^{o}C), a tiny amount of oxygen would aid to burn them away. Nevertheless, in comparison with curve a and b in Fig. 6, they indicate that the coating of PDA protects and improves the thermal stability of the PS spheres, in other words, the decomposition of the PS spheres was retarded to 400 ^{o}C and 26% of the residue was preserved after the rise of the temperature to 450 ^{o}C due to the protection layer of PDA. On the other hand, the layer of PDA assisted the deposition of silver nanoparticles, which, consequently, increased the weight percent of the residue from the organic and inorganic composite PS/Ag particles after sintering. The curves (c-e) in Fig. 6 clearly indicate that the more silver nanoparticles were loaded, the more residues were left over, which is consistent with the results reported in ref.58.

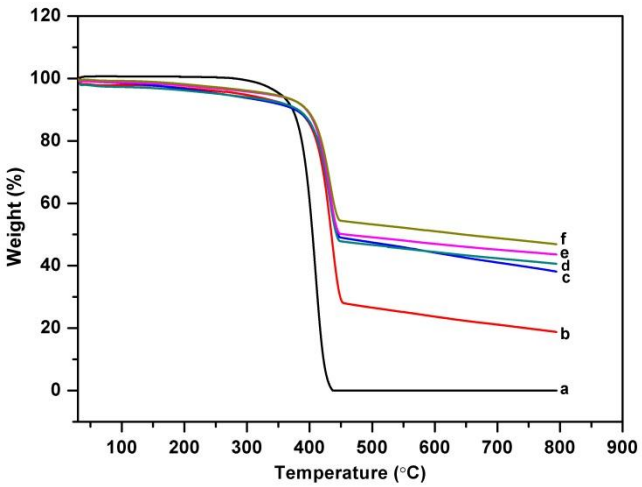

Fig.6 Thermogravimetric analysis (TGA) curves of (a) PS spheres, (b) PS/PDA composite spheres and (c-f) PS/Ag nanocomposite particles prepared by using various concentrations of $[Ag(NH_3)_2]^+$ ions: (c) 1.2×10^{-2} mol/L; (d) 2.3×10^{-2} mol/L; (e) 4.7×10^{-2} mol/L and (f) 9.4×10^{-2} mol/L. PS/PDA composite particles: 0.1 g ; $[Ag(NH_3)_2]^+$ ions: 50 mL of aqueous solution; Time: 1 h; Temperature: room temperature.

Therefore, all evidences demonstrate that the polydopamine coatings on the PS spheres can successfully assist binding with $[Ag(NH_3)_2]^+$ ions and spontaneously reduce the $[Ag(NH_3)_2]^+$ ions to Ag nanoparticles. Compared with those traditional methods for preparing Ag-based nanocomposite spheres by adding $SnCl_2$, palladium as surface activating materials or using certain reagents as reducing agents,[28-30, 67] this polydopamine-assisted electroless Ag metallization procedure is a simple, mild and environmentally friendly route for the synthesis of the Ag-based nanocomposite spheres, because there no additional reducing agents and other toxic reagents are used in this process.

3.4 Reaction mechanism of PS/Ag nanocomposite particles by polydopamine-assisted electroless Ag metallization

On the basis of all the experimental results and discussions, a possible reaction mechanism of PS/Ag nanocomposite particles formed by polydopamine-assisted electroless Ag metallization is described in Scheme 1. Those monodisperse PS template spheres were first dispersed in the aqueous Tris-HCl buffer solution, and then, mixed with dopamine (2 mg of dopamine per milliliter of 10 mM Tris-HCl, pH = 8.5). Subsequently, the self-polymerization of dopamine was followed and carried out to form a thin adherent polydopamine coating on the surfaces of the PS template spheres under a weakly alkaline aqueous environment (pH = 8.5). As mentioned, the as-formed surface-adherent polydopamine coatings are abundant of active catechol and amine groups, which can facilitate the secondary reaction or decoration nanoparticles onto the surface. Therefore, with the addition of PS/PDA composite spheres into the freshly prepared $[Ag(NH_3)_2]^+$ ions aqueous solution, these silver precursor-$[Ag(NH_3)_2]^+$ ions can be absorbed onto the surfaces of the PS/PDA composite spheres by those active catechol and amine groups of the polydopamine coatings, and are *in situ* reduced into metallic silver nanoparticles. The formed Ag nanoparticles are home positioned.

In this approach of polydopamine-assisted electroless Ag metallization, polydopamine coatings provide an excellent platform to *in situ* bind and reduce silver precursor- $[Ag(NH_3)_2]^+$ ions into metallic Ag nanoparticles because of their abundant active catechol and amine groups. Neither additional reducing and toxic reagents nor special surface modification of the template are needed in this procedure. Moreover, the coverage

and the size of the Ag nanoparticles on the surface of PS/PDA composite spheres can be easily tailored through the adjustment of the concentration of the silver precursor.

3.5 Antibacterial properties of PS/Ag nanocomposite particles

Usually, silver and silver based nanomaterials are well known with their strong biocidal activities for a wide range of bacteria.[9, 14-16, 18, 68] Concerning the prospective applications of the PS/Ag nanocomposite particles as antibacterial agents, both *Escherichia coli* (Gram-negative bacteria) and *Staphylococcus aureus* (Gram-positive bacteria) were used as the bacterium models to investigate the antibacterial properties of the PS/Ag nanocomposite particles in the present work.

First, the bacterial inhibition growth curves were used to investigate the antibacterial properties of the PS/Ag nanocomposite particles. In this process, PS/Ag nanocomposite particles prepared at the concentration of 4.7×10^{-2} mol/L of $[Ag(NH_3)_2]^+$ ions was chosen as the typical antibacterial agent for antibacterial investigation. The diluted solutions of the PS/Ag nanocomposite particles were firstly incubated with *Escherichia coli* and *Staphylococcus aureus*, respectively, and then, the bacterial proliferation was monitored by the optical density at 600 nm (O.D. 600) based on the turbidity of the cell suspension within 10 h. As shown in Fig. 7, compared to the control groups, the growth rates of the bacteria (*Escherichia coli* and *Staphylococcus aureus*) in the presence of 5 μg /mL of PS/Ag nanocomposite particles were both slightly retarded. Remarkably, the growths of the bacteria were completely inhibited during the whole 10 h of culture period when the minimum inhibition concentrations (MIC) of the PS/Ag nanocomposite particles was 20 μg/mL for *Escherichia coli* and 40 μg/mL for *Staphylococcus aureus*, respectively. The results have qualitatively illustrated that the PS/Ag nanocomposite particles can effectively inhibit both growth of *Escherichia coli* and *Staphylococcus aureus*, while *Escherichia coli* (Gram-positive bacteria) showed more sensitive to the PS/Ag nanocomposite particles than *Staphylococcus aureus* (Gram-negative bacteria). So as to further confirm which components in the PS/Ag nanocomposite particles play the key role for the antibacterial activities. We set pure PS/PDA composite spheres as the control group for both strains. As results showing, only pure PS/PDA composite spheres cannot inhibit both strains of the bacterial growth. This result indicates that the antibacterial activities of the PS/Ag nanocomposite particles are mainly from the Ag nanoparticles attached on the surfaces of the PS/PDA spheres. Also the possible reasons for the different sensitive of those strains to the PS/Ag nanocomposite particles may ascribe to the fact that the membrane of the Gram-positive bacteria is thicker and more stable than that of the Gram-negative bacteria.[69] Moreover, Gram-positive bacteria generally show less susceptible to the antibacterial agents containing silver ion than Gram-negative species. [70]

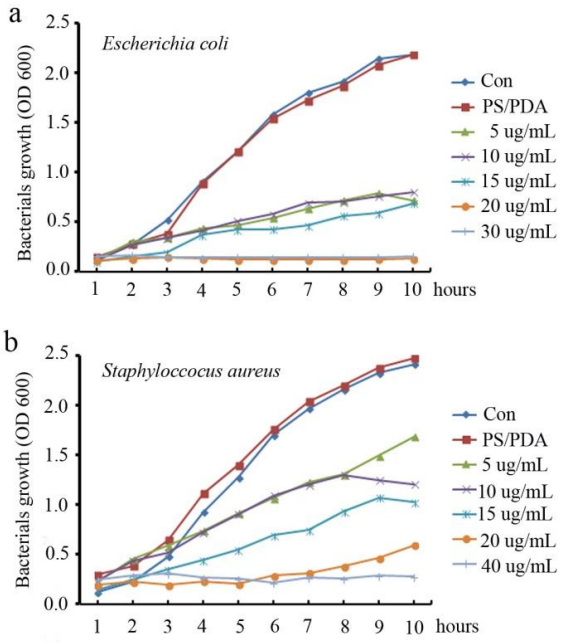

Fig.7 Bacterial growth curves in LB media with PS/Ag nanocomposite particles. Different concentrations of PS/Ag nanocomposite particles were added to the culture of *Escherichia coli* (a) and *Staphylococcus aureus* (b). The growth of the bacteria was measured by a judgment of the O.D. at the wavelength of 600 nm. The initial addition of the PS/Ag nanocomposite particles to the LB bacterium suspension was regarded as the starting point.

In addition, the antibacterial properties of the PS/Ag nanocomposite particles were also compared with the reported results. In literatures, for the *Escherichia coli* system, the minimum inhibition concentrations (MIC) of silver-based materials were 7.12, 62.5, 70, 130.2 and 12.5 μg/mL corresponding to Ag-polymer, Ag-SiO_2, Ag-Fe_3O_4, Ag-TiO_2, and Ag-carbonaceous materials, while, in the *Staphylococcus aureus*, the MIC values became to 3.56, 250, 60 and 250 μg/mL, respectively.[71-75] Although the experimental conditions may be variable in one system to others, an apparently enhanced

antibacterial activity of these PS/Ag nanocomposite particles can be concluded.

To further confirm the effect of the PS/Ag nanocomposite particles on bacterial viabilities, live/dead bacterial cell fluorescence stain assay was employed in the present study. The bacterial cells of both strains were incubated for 12 h with 15 μg/mL of PS/Ag nanocomposite particles. Later, cells were harvested for staining. Blue fluorescent dye was used to stain both live/dead cells, while red fluorescent dye only stained dead cells. As Fig. 8 showing, the majority of the cells show a strong red fluorescence in both types of strains. This indicates both strains of the cells showed a poor-medium survivability in the environment with PS/Ag nanocomposite particles.[70] And further, a higher percentage of the dead cells (red fluorescence) was found in *Escherichia coli* groups in comparing with that in *Staphylococcus aureus* group, which is consistent with that observed in antibacterial activities assays.

All the above results have illustrated that PS/Ag nanocomposite particles were able to effectively inhibit the growth of both *Escherichia coli* (Gram-negative bacteria) and *Staphylococcus aureus* (Gram-positive bacteria) growth. The antibacterial activities mainly impute to the Ag nanoparticles attached on the surfaces of the PS/Ag nanocomposite particles. In addition, their antibacterial properties were also compared with those from commercial product kanamycin. The as-synthesized PS/Ag nanocomposite particles showed a comparable antibacterial ability with kanamycin against both *Escherichia coli* and *Staphylococcus aureus* (see Supplementary Information).

On the basis of our experimental results and discussion combining with the knowledge in the literatures,[9, 14, 18, 72, 76, 77] the enhanced antibacterial activities of these PS/Ag nanocomposite particles are probably ascribed to the Ag nanoparticles attached. The antibacterial activities can be explained by the following possible bactericidal mechanisms: (1) Due to the abundance of sulfur-containing proteins on the bacterial cell membrane, the silver-based materials themselves can directly react with those sulfur-containing proteins inside or outside the cell membrane of the bacteria, which straightly causes the structural changes or functional damages to the cell membrane of the bacteria, and further affect the viability of the bacterial cells;[9, 14] (2) The released Ag ions from silver-based materials are also able to deactivate microorganism cells to death by interacting with the disulfide or sulfhydrol groups of the enzymes, and further causing the structural changes and destroying the metabolic process of bacterial cells.[15, 16]

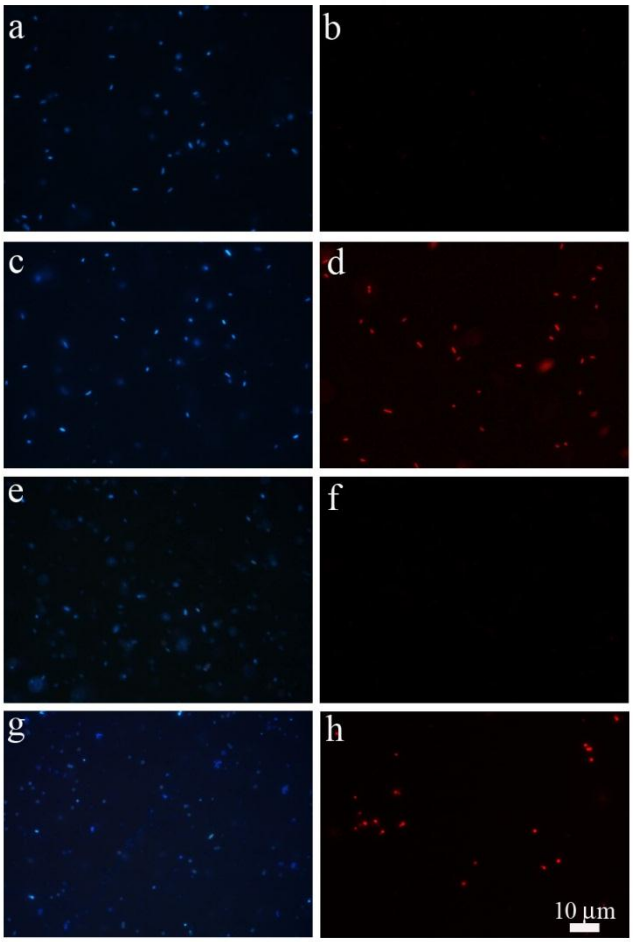

Fig.8 Fluorescent images of the antibacterial activities of the PS/Ag nanocomposite particles against *Escherichia coli* (a-d) and *Staphylococcus aureus*(e-h). (a, b, e and f) Control groups for *Escherichia coli* and *Staphylococcus aureus*, respectively; (c, d, g and h) PS/Ag nanocomposite particles treated groups for *Escherichia coli* and *Staphylococcus aureus*, respectively. *Escherichia coli* and *Staphylococcus aureus* strains were incubated for 12 h in LB medium with 15 μg/mL of PS/Ag nanocomposite particles. The red fluorescent dye stained only dead cells, while the blue fluorescent dye stained both live and dead cells. The scale bar is 10 μm for all the images.

3.6 *In Vitro* cytotoxicity of PS/Ag nanocomposite particles

To consider PS/Ag nanocomposite particles as promising potential antibacterial materials for future biomedical applications, the cytotoxicity of PS/Ag nanocomposite particles should be evaluated at first, which is one of the primary concerns in the use of these silver-based nanomaterials as antimicrobial agent *in vivo* for the clinical therapeutics.

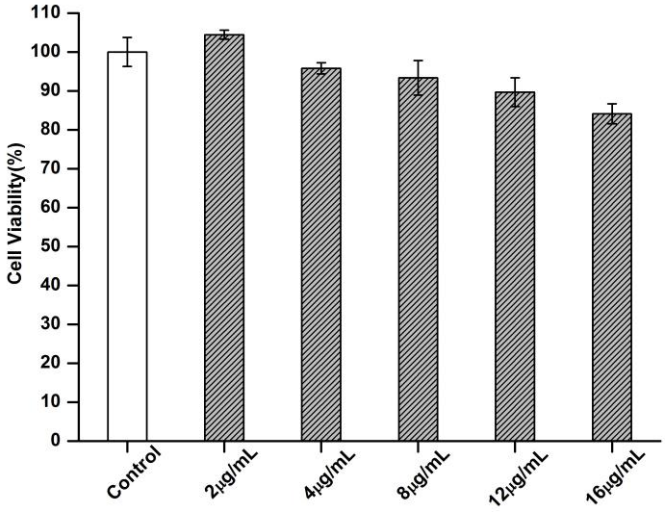

Fig.9 *In vitro* cytotoxicity (CCK-8 assay) of PS/Ag nanocomposite particles against HEK293T human embryonic kidney cells after incubation for 24 h at 37 ^{o}C.

First, PS/Ag nanocomposite particles that prepared at the concentration of 4.7×10^{-2} mol/L of $[Ag(NH_3)_2]^+$ ions, were chosen as the typical sample for the *in vitro* cytotoxicity assay. These as-synthesized PS/Ag nanocomposite particles dispersed in the HEK293T human embryonic kidney cells incubation with the final concentrations ranging from 0 to 16 μg/mL were used to treat with cells and incubated at 37^{o}C for 24 h. Subsequently, the *in vitro* cytotoxicity of PS/Ag nanocomposite particles was evaluated referenced to the pure HEK293T human embryonic kidney cells by using the Cell Counting Kit-8(CCK-8) assay. Basically, CCK-8 allows sensitive colorimetric assays for the determination of cell viability in cell proliferation and cytotoxicity assays.[71, 78] Moreover, considering the optical interference from the Ag nanoparticles on the surfaces of PS/PDA composite particles, the absorbance background at 450 nm (initial time after CCK-8 was added) was removed from the absorbance after 2 h incubation with CCK-8. As shown in Fig.9, the PS/Ag nanocomposite particles did not show a significant cytotoxicity against the HEK293T human embryonic kidney cells. More than 84.14% of the cells were still viable even a high concentration of PS/Ag nanocomposite particles (16 μg/mL) was used after the incubation for 24 h at 37 ^{o}C. These results indicate that PS/Ag nanocomposite particles have a reasonably good cytocompatibility to human cells. As shown, this *in vitro* cytotoxicity assay of the PS/Ag nanocomposite particles gave an indicator of their toxicities *in vivo*. Thus, the further *in vivo* use of these PS/Ag nanocomposite particles is possible and attractive.

4. Conclusions

In summary, we present a simple, mild and environmentally friendly approach to prepare PS/Ag nanocomposite particles through the polydopamine-assisted electroless Ag metallization procedure. Neither additional reducing agents nor toxic reagents are needed in this procedure. TEM, SEM and XPS results have demonstrated the formation of the PS/Ag nanocomposite particles, and XRD patterns have indicated that Ag nanoparticles have been crystalized. Moreover, the controlled size and morphology of the Ag nanoparticles on the surface of the PS spheres can be facilely tuned by adjusting the concentration of the silver precursor-$[Ag(NH_3)_2]^+$ ions. And, the preliminary antibacterial assays indicate that these PS/Ag nanocomposite particles have exhibited extraordinary antibacterial activities against Escherichia coli (Gram-negative bacteria) and *Staphylococcus aureus* (Gram-positive bacteria), which is comparable with commercial. Moreover, the *in vitro* cytotoxicity assays indicate that PS/Ag nanocomposite particles have a good cytocompatibility against the HEK293T human embryonic kidney cells. Based on these advantages, we believe these PS/Ag nanocomposite particles produced by this environmentally friendly method are promising potential antibacterial materials for future biomedical applications.

Moreover, this environmentally friendly method based on polydopamine-assisted electroless metallization can also present a new paradigm to deposit different metallic (Au, Pd, Pt, Cu and Ni, etc) onto various kinds of materials surfaces, including polymers, metals and ceramics. On the basis of this technique, many kinds of materials coated with various metal nanoparticles can be possibly achieved, and which are expected to be promising nanocomposite materials for biomedical and environmental applications.

Acknowledgements

We acknowledge the National Natural Science Foundation of China (No.51203087), the Natural Science Basic Research Plan in Shaanxi Province of China (No.2013JQ2006), the Fundamental Research Funds for the Central Universities (No.GK201102003) the Scientific Research Foundation for the Returned Overseas Chinese Scholars, State Education Ministry and the National Key Technology R&D Program of China (No.2012BAD12B03) for financial support. We also thank Dr. Min Chen and Miss. Chenyu Ye (Department of

Materials Science and the Advanced Coatings Research Center of China Educational Ministry, Fudan University, China) for the help of the schematic diagram drawed in this work.

Notes and references

1 V. K. Sharma, R. A. Yngard and Y. Lin, *Adv. Colloid Interface Sci.*, 2009, **145**, 83-96.
2 M. Rai, A. Yadav and A. Gade, *Biotechnol. Adv.*, 2009, **27**, 76-83.
3 C. N. Lok, C. M. Ho, R. Chen, Q. Y. He, W. Y. Yu, H. Sun, P. K. H. Tam, J. F. Chiu and C. M. Che, *J. Biol. Inorg. Chem.*, 2007, **12**, 527-534.
4 C. Marambio-Jones and E. M. V. Hoek, *J. Nanopart. Res.*, 2010, **12**, 1531-1551.
5 M. Heinlaan, A. Ivask, I. Blinova, H. C. Dubourguier and A. Kahru, *Chemosphere*, 2008, **71**, 1308-1316.
6 G. Applerot, A. Lipovsky, R. Dror, N. Perkas, Y. Nitzan, R. Lubart and A. Gedanken, *Adv. Funct. Mater.*, 2009, **19**, 842-852.
7 Y. H. Kim, D. K. Lee, H. G. Cha, C. W. Kim, Y. C. Kang and Y. S. Kang, *J. Phys. Chem. B*, 2006, **110**, 24923-24928.
8 Y. Y. Zhao, Y. Tian, Y. Cui, W. W. Liu, W. S. Ma and X. Y. Jiang, *J. Am. Chem. Soc.*, 2010, **132**, 12349-12356.
9 Q. L. Feng, J. Wu, G. Q. Chen, F. Z. Cui, T. N. Kim and J. O. Kim, *J. Biomed. Mater. Res.*, 2000, **52**, 662-668.
10 S. Pal, Y. K. Tak and J. M. Song, *Appl. Environ. Microbiol.*, 2007, **73**, 1712-1720.
11 N. R. Panyala, E. M. Pena-Mendez and J. Havel, *J.Appl.Biomed*, 2008, **6**, 117-129.
12 P. V. AshaRani, G. L. K. Mun, M. P. Hande and S. Valiyaveettil, *ACS Nano*, 2009, **3**, 279-290.
13 M. Bosetti, A. Masse, E. Tobin and M. Cannas, *Biomaterials*, 2002, **23**, 887-892.
14 H. Y. Lee, H. K. Park, Y. M. Lee, K. Kim and S. B. Park, *Chem. Commun.*, 2007, 2959-2961.
15 Y. Matsumura, K. Yoshikata, S. Kunisaki and T. Tsuchido, *Appl. Environ. Microbiol.*, 2003, **69**, 4278-4281.
16 A. Gupta, M. Maynes and S. Silver, *Appl. Environ. Microbiol.*, 1998, **64**, 5042-5045.
17 A. Panacek, L. Kvitek, R. Prucek, M. Kolar, R. Vecerova, N. Pizurova, V. K. Sharma, T. Nevecna and R. Zboril, *J. Phys. Chem. B*, 2006, **110**, 16248-16253.
18 J. R. Morones, J. L. Elechiguerra, A. Camacho, K. Holt, J. B. Kouri, J. T. Ramirez and M. J. Yacaman, *Nanotechnology*, 2005, **16**, 2346-2353.
19 C. Baker, A. Pradhan, L. Pakstis, D. J. Pochan and S. I. Shah, *J. Nanosci. Nanotechnol.*, 2005, **5**, 244-249.
20 A. S. Kumbhar and G. Chumanov, *Chem. Mater.*, 2009, **21**, 2835-2839.
21 J. M. Li, W. F. Ma, C. A. Wei, J. Guo, J. Hu and C. C. Wang, *J. Mater. Chem.*, 2011, **21**, 5992-5998.
22 Z. W. Deng, M. Chen and L. M. Wu, *J. Phys. Chem. C*, 2007, **111**, 11692-11698.
23 P. Dallas, J. Tucek, D. Jancik, M. Kolar, A. Panacek and R. Zboril, *Adv. Funct. Mater.*, 2010, **20**, 2347-2354.
24 B. S. Necula, L. E. Fratila-Apachitei, S. A. J. Zaat, I. Apachitei and J. Duszczyk, *Acta Biomater.*, 2009, **5**, 3573-3580.
25 P. C. Ma, B. Z. Tang and J. K. Kim, *Carbon*, 2008, **46**, 1497-1505.
26 K. Y. Chun, Y. Oh, J. Rho, J. H. Ahn, Y. J. Kim, H. R. Choi and S. Baik, *Nat. Nanotechnol.*, 2010, **5**, 853-857.
27 R. Pasricha, S. Gupta and A. K. Srivastava, *Small*, 2009, **5**, 2253-2259.
28 I. Washio, Y. Xiong, Y. Yin and Y. Xia, *Adv.Mater.*, 2006, **18**, 1745-1749.
29 J. L. Zhang, B. X. Han, J. C. Liu, X. G. Zhang, J. He, Z. M. Liu, T. Jiang and G. Y. Yang, *Chem.Eur.J.*, 2002, **8**, 3879-3883.
30 A. Henglein and M. Giersig, *J. Phys. Chem. B*, 1999, **103**, 9533-9539.
31 J. H. Zhang, J. B. Liu, S. Z. Wang, P. Zhan, Z. L. Wang and N. B. Ming, *Adv. Funct. Mater.*, 2004, **14**, 1089-1096.
32 Y. Kobayashi, V. Salgueirino-Maceira and L. M. Liz-Marzan, *Chem. Mater.*, 2001, **13**, 1630-1633.
33 H. L. Cao, X. Y. Liu, F. H. Meng and P. K. Chu, *Biomaterials*, 2011, **32**, 693-705.
34 H. Lee, S. M. Dellatore, W. M. Miller and P. B. Messersmith, *Science*, 2007, **318**, 426-430.
35 H. Lee, B. P. Lee and P. B. Messersmith, *Nature*, 2007, **448**, 338-341.
36 S. H. Yang, S. M. Kang, K.B. Lee, T. D. Chung, H. Lee and I. S. Choi, *J. Am. Chem. Soc.*, 2011, **133**, 2795-2797.
37 J. Cui, Y. Wang, A. Postma, J. Hao, L. Hosta-Rigau and F. Caruso, *Adv. Funct. Mater.*, 2010, **20**, 1625-1631.
38 Y. Liu, K. Ai, J. Liu, M. Deng, Y. He and L. Lu, *Adv. Mater.*, 2013, **25**, 1353-1359.
39 M. E. Lynge, R. van der Westen, A. Postma and B. Stadler, *Nanoscale*, 2011, **3**, 4916-4928.
40 Z. W. Deng, M. Chen, G. X. Gu and L. M. Wu, *J. Phys. Chem. B*, 2008, **112**, 16-22.
41 L. Guo, Q. Liu, G. Li, J. Shi, J. Liu, T. Wang and G. Jiang, *Nanoscale*, 2012, **4**, 5864-5867.
42 J. Yan, L. P. Yang, M. F. Lin, J. Ma, X. H. Lu and P. S. Lee, *Small*, 2013, **9**, 596-603.
43 M. Sureshkumar, P.N. Lee and C.K. Lee, *J. Mater. Chem.*, 2011, **21**, 12316-12320.
44 Z. W. Deng, Z. P. Zhen, X. X. Hu, S. L. Wu, Z. S. Xu and P. K. Chu, *Biomaterials*, 2011, **32**, 4976-4986.
45 Z. W. Deng, M. Chen, S. X. Zhou, B. You and L. M. Wu, *Langmuir*, 2006, **22**, 6403-6407.
46 M. Chen, L. M. Wu, S. X. Zhou and B. You, *Adv. Mater.* , 2006, **18**, 801-806.
47 M. Chen, J. Zhou, L. Xie, G. X. Gu and L. M. Wu, *J. Phys. Chem. C*, 2007, **111**, 11829-11835.
48 X. Ding, S. Zhou, G. Gu and L. Wu, *J. Mater. Chem.*, 2011, **21**, 6161-6164.
49 B. Peng, M. Chen, S. X. Zhou, L. M. Wu and X. H. Ma, *J. Colloid Interface Sci.*, 2008, **321**, 67-73.
50 B. Peng, E. van der Wee, A. Imhof and A. van Blaaderen, *Langmuir*, 2012, **28**, 6776-6785.
51 X. Hu, Y. Wang and B. Peng, *Chem.Asian J.*, 2014, **9**, 319-327.
52 B. Peng, H. R. Vutukuri, A. van Blaaderen and A. Imhof, *J. Mater. Chem.*, 2012, **22**, 21893-21900.
53 B. Peng, A. van Blaaderen and A. Imhof, *Acs Appl Mater Inter*, 2013, **5**, 4277-4284.

54 B. Peng, F. Smallenburg, A. Imhof, M. Dijkstra and A. van Blaaderen, *Angew.Chem.Int.Ed.*, 2013, **52**, 6709-6712.
55 C. Wu, W. Fan, J. Chang and Y. Xiao, *J. Mater. Chem.*, 2011, **21**, 18300-18307.
56 T. Zeng, X. L. Zhang, Y. R. Ma, H. Y. Niu and Y. Q. Cai, *J. Mater. Chem.*, 2012, **22**, 18658-18663.
57 J. Jiang, L. Zhu, L. Zhu, B. Zhu and Y. Xu, *Langmuir*, 2011, **27**, 14180-14187.
58 W. Wang, Y. Jiang, S. Wen, L. Liu and L. Zhang, *J. Colloid Interface Sci.*, 2012, **368**, 241-249.
59 A. Okada, D. Nagao, H. Ishii and M. Konno, *Soft Matter*, 2012, **8**, 3442-3445.
60 D. Nagao, T. Ohta, H. Ishii, A. Imhof and M. Konno, *Langmuir*, 2012, **28**, 17642-17646.
61 A. F. Demirörs, A. van Blaaderen and A. Imhof, *Chem.Mater.*, 2009, **21**, 979-984.
62 V. K. LaMer and R. H. Dinegar, *J. Am. Chem. Soc.*, 1950, **72**, 4847-4854.
63 T. Sugimoto, ed., *Monodispersed particles*, Elsevier, Amsterdam, 2001.
64 G. Schmid, *Nanoparticles: From Theory to Application*, Wiley-VCH, Weinheim, 2004.
65 C. Li, L. Luo and G. Xiong, *Chin. J. Catal.*, 2009, **30**, 1058-1062.
66 J. F. Yan, Z. Y. Zhang, T. G. You, W. Zhao, J. N. Yun and F. C. Zhang, *Chin. Phys. B*, 2009, **18**, 4552-4557.
67 C. E. Hoppe, M. Lazzari, I. Pardiñas-Blanco and M. A. López-Quintela, *Langmuir*, 2006, **22**, 7027-7034.
68 D. Lee, R. E. Cohen and M. F. Rubner, *Langmuir*, 2005, **21**, 9651-9659.
69 J. Njagi, M. M. Chernov, J. C. Leiter and S. Andreescu, *Anal. Chem.*, 2010, **82**, 989-996.
70 E. Fortunati, S. Mattioli, L. Visai, M. Imbriani, J. L. G. Fierro, J. M. Kenny and I. Armentano, *Biomacromolecules*, 2013, **14**, 626-636.
71 K. Zou, Q. Liu, J. Chen and J. Du, *Poly.Chem.*, 2014, **5**, 405-411.
72 S. Egger, R. P. Lehmann, M. J. Height, M. J. Loessner and M. Schuppler, *Appl. Environ. Microbiol.*, 2009, **75**, 2973-2976.
73 P. Gong, H. Li, X. He, K. Wang, J. Hu, W. Tan, S. Zhang and X. Yang, *Nanotechnology*, 2007, **18**, 285604.
74 N. Niño-Martínez, G. A. Martínez-Castañón, A. Aragón-Piña, F. Martínez-Gutierrez, J. R. Martínez-Mendoza and F. Ruiz, *Nanotechnology*, 2008, **19**, 065711.
75 W. P. Xu, L. C. Zhang, J. P. Li, Y. Lu, H. H. Li, Y. N. Ma, W. D. Wang and S. H. Yu, *J. Mater. Chem.*, 2011, **21**, 4593-4597.
76 J. Z. Ma, J. T. Zhang, Z. G. Xiong, Y. Yong and X. S. Zhao, *J. Mater. Chem.*, 2011, **21**, 3350-3352.
77 Z. Zhang, J. Zhang, B. Zhang and J. Tang, *Nanoscale*, 2013, **5**, 118-123.
78 J. Park, D. H. Lim, H. J. Lim, T. Kwon, J. Choi, S. Jeong, I. H. Choi and J. Cheon, *Chem. Commun.*, 2011, **47**, 4382-4384.

Table of contents entry

Mussel inspired polydopamine coating-assisted electroless Ag metallization procedure was presented to prepare PS/Ag nanocomposite particles with enhanced antibacterial activities.